AGU PUBLICATIONS

JGR

Journal of Geophysical Research: Atmospheres

RESEARCH ARTICLE
10.1002/2014JD022310

Key Points:
- Comparison of several methods to estimate LW under cloudy skies is presented
- Using synthetic profiles, estimated CBH, LW is approached within 7 W m^{-2} (1 SD)
- CRE at the surface decreases with CBH at 4–5 W m^{-2}/km in a midlatitude site

Correspondence to:
A. Viúdez-Mora,
toni.v.mora@nasa.gov

Citation:
Viúdez-Mora, A., M. Costa-Surós, J. Calbó, and J. A. González (2015), Modeling atmospheric longwave radiation at the surface during overcast skies: The role of cloud base height, *J. Geophys. Res. Atmos.*, *120*, 199–214, doi:10.1002/2014JD022310.

Received 14 JUL 2014
Accepted 6 DEC 2014
Accepted article online 11 DEC 2014
Published online 8 JAN 2015

Modeling atmospheric longwave radiation at the surface during overcast skies: The role of cloud base height

A. Viúdez-Mora[1], M. Costa-Surós[2], J. Calbó[2], and J. A. González[2]

[1]NASA Langley Research Center, Science Mission Directorate, Hampton, Virginia, USA, [2]Group of Environmental Physics, University of Girona, GIRONA, Spain

Abstract The behavior of the atmospheric downward longwave radiation at the surface under overcast conditions is studied. For optically thick clouds, longwave radiation depends greatly on the cloud base height (CBH), besides temperature and water vapor profiles. The CBH determines the cloud emission temperature and the air layers contributing to the longwave radiation that reaches the surface. Overcast situations observed at Girona (NE Iberian Peninsula) were studied by using a radiative transfer model. The data set includes different seasons, and a large range of CBH (0–5000 m). The atmosphere profiles were taken from the European Center for Medium-Range Weather Forecast analysis. The CBH was determined from ceilometer measurements and also estimated by using a suitable method applied to the vertical profile of relative humidity. The agreement between calculations and pyrgeometer measurements is remarkably good (1.6 ± 6.2 W m^{-2}) if the observed CBH is used; poorer results are obtained with the estimated CBH (4.3 ± 7.0 W m^{-2}). These results are better than those obtained from a simple parameterization based upon ground-level data (1.1 ± 11.6 W m^{-2}), which can be corrected by adding a term that takes into account the CBH (-0.1 ± 7.3 W m^{-2}). At this site, the cloud radiative effect (CRE) at the surface lies in the range 50–80 W m^{-2}, has a clear seasonal behavior (higher CRE in winter), and depends upon the CBH. For the cold and the warm seasons, CRE decreases with CBH at a rate of -5 and -4 W m^{-2}/km, respectively. Results obtained for other climates (subarctic and tropical) are also presented.

1. Introduction

The radiative processes involved in the global energy budget are, among other components, key factors to understanding the climate and the current climate change. The atmospheric downward longwave (3 to 100 μm) radiation is one of the radiative fluxes taking part of the energy budget. This radiation is emitted by the atmosphere itself, mainly by H_2O, CO_2, and O_3 molecules, as well as by aerosol, water droplets, and ice crystals in clouds and fog. Global mean longwave radiation reaching the terrestrial surface has a relatively small year-to-year variation, but it is strongly related with enhanced greenhouse effect by the anthropogenic greenhouse gases and also with cloud cover [*Wild et al.*, 1997; *Marty et al.*, 2003]. Clouds are global in nature; recent studies show that clouds regularly cover almost 68% of the Earth [*Stubenrauch et al.*, 2013]. Therefore, clouds have a strong modulating influence on the radiative exchange, constituting the most important factor determining the transmission of solar energy in the atmosphere as well as the amount of infrared energy radiated toward the space and the surface (for an overview on this matter, see *Arking* [1991]). The emission by clouds increases the longwave irradiance received at the surface, mainly in the atmospheric window (i.e., the wave band lacking of gaseous emissions, between 8 and 12 μm).

The important role of clouds in the climate system, and specifically in the radiation balance, can be described by introducing the cloud radiative effect (CRE) concept, which is usually defined as the change in radiative fluxes at the top of the atmosphere when clouds are present relative to cloud-free situations [*Chylek and Wong*, 1998; *Chen et al.*, 2000; *Ramanathan et al.*, 1989]. The global CRE at the top of the atmosphere is estimated about -20 W m^{-2} [*Loeb et al.*, 2009], which results from a negative effect in the shortwave (-50 W m^{-2}) and a positive counterpart in the longwave ($+30$ W m^{-2}). The decadal change of these amounts and the regional and local details still present some uncertainty, despite the contribution of projects such as the Earth Radiation Budget Experiment and the Clouds and the Earth's Radiant Energy System (CERES) [*Stephens and Webster*, 1980; *Arking*, 1991; *Wielicki et al.*, 1996; *Stephens et al.*, 2012; *Boucher et al.*, 2013]. The

CRE concept may also be applied to the radiative fluxes at the surface, as a measure of the contribution of clouds in the downward component of the energy budget. For the longwave band, *Bréon et al*. [1991] evaluated this effect, using modeling and measurements, to be in the range from 40 to 50 W m^{-2}. In any case, important efforts are being devoted to reduce the uncertainties associated to cloud effects on radiation fluxes; many of the most recent global studies make use of the comprehensive characterization of clouds provided by instruments on the A-Train Constellation of satellites [e.g., *Kato et al*., 2011].

The downward longwave radiation incident onto the surface can be routinely measured by pyrgeometers. Specifically, these instruments measure the irradiance (radiation flux) on a horizontal surface, which will be denoted here as LW↓. When correctly installed and accurately calibrated, measurements may reach an uncertainty of 1.5 W m^{-2} (about 0.5%) for clear-sky nighttime measurements, a remarkable improvement from the early pyrgeometers, that at 1990s had still uncertainties around 10% (corresponding to 30–40 W m^{-2}) [*Philipona et al*., 2001].

When direct measurements are unavailable, several methods can be used to estimate LW↓ (for a review of observations and satellite and reanalyses estimations of LW↓, see *Wang and Dickinson* [2013]). The simplest methods are parameterizations that are based on the empirical relationship between LW↓ (for clear-sky conditions) and screen-level variables (meaning variables taken at the standard level of meteorological measurements, i.e., 1.5 m above the ground) that was first presented by *Ångström* [1915]. The starting point is that the atmosphere can be considered as a grey body, so LW↓ is determined by the bulk emissivity $\varepsilon_{\mathrm{atm}}$ and the effective temperature of the overlying atmosphere T_{atm}. Since it is difficult to determine both the bulk emissivity and the effective temperature of a vertical column of the atmosphere [*Crawford and Duchon*, 1999], LW↓ is usually estimated, for cloudless sky conditions, by using the screen-level air temperature T_a and the vapor pressure e. Thus, we have the following:

$$\mathrm{LW}\downarrow = \varepsilon_{\mathrm{atm}}(T_a, e)\sigma T_a^4 \tag{1}$$

where σ is the Stefan-Boltzmann constant. Different expressions have been suggested to estimate $\varepsilon_{\mathrm{atm}}(T_a, e)$ for the cloudless atmosphere. When these simple estimations of LW↓ are compared with measurements, the results are satisfactory at least when applied to the site(s) where they were developed but also quite correct when applied to different locations [*Iziomon et al*., 2003; *Viúdez-Mora et al*., 2009]. Some recent works have suggested the use of an "effective atmospheric boundary layer temperature" or an "effective radiating temperature" that in some way takes into account the vertical profile of temperature (including inversions) in the lowest atmospheric levels to obtain better estimations of LW↓ [*Gröbner et al*., 2009; *Wacker et al*., 2013]. However, measured longwave radiation is needed to calculate these effective temperatures so the practical application is limited when no measurements are available.

The effect of clouds can be implemented in these parameterizations by modifying the bulk emissivity depending on the cloud fraction and/or type. Since clouds behave approximately as a blackbody, the most relevant parameter (besides the amount of clouds present, i.e., the cloud fraction) for the downward radiation is the temperature of its lower boundary (the cloud base). This temperature is closely related to the cloud base height and therefore to cloud type. Thus, equation (1) can be generalized in presence of clouds as follows:

$$\mathrm{LW}\downarrow = \varepsilon_{\mathrm{atm}}\left(f_{\mathrm{cld}}, T_a, e\right)\sigma T_a^4 \tag{2}$$

where f_{cld} stands for some properties of clouds. Very often the cloud effect is expressed as a cloud modification factor (CMF) applied to the clear sky downward longwave radiation ($\mathrm{LW_{cs}}\downarrow$):

$$\mathrm{LW}\downarrow = \mathrm{CMF}\ \ \mathrm{LW_{cs}}\downarrow = \mathrm{CMF}\varepsilon_{\mathrm{atm}}(T_a, e)\sigma T_a^4 \tag{3}$$

Several parameterizations for either CMF or $\varepsilon_{\mathrm{atm}}(f_{\mathrm{cld}}, T_a, e)$, which mostly include only the effect of cloud fraction, have been proposed in the past [*Jacobs*, 1978; *Maykut and Church*, 1973; *Sugita and Brutsaert*, 1993; *Konzelmann et al*., 1994; *Crawford and Duchon*, 1999]. Other authors have developed parameterizations of longwave radiative properties of water or ice clouds; these parameterizations try to describe the radiative properties of clouds using simple relationships between optical and liquid-ice properties of cloud droplets. *Stephens* [1978] scheme was based on the parameterization of cloud effective emissivity as a function of the liquid water path (LWP). This allowed the calculation of broadband infrared fluxes and also the cooling rates within the cloud. *Liou and Wittman* [1979] parameterized the infrared reflectivity, transmissivity, and

emissivity of cirrus clouds in terms of the cloud vertical ice content; *Fu and Liou* [1993] extended this study by considering the size distribution, and different shapes, of the ice crystals.

Radiative transfer models (RTMs) use more rigorous formalism to calculate cloud emittance at any wavelength for a given size distribution of spherical particles. Although such detailed calculations are time consuming and are unsuitable to be used in climate or numerical weather prediction models [*Chylek et al*., 1992], it is expected that they can reach (when some input conditions are conveniently included) the best agreement with measurements. In this sense, *Wacker et al*. [2011] describe a study of the longwave CRE of stratus clouds based upon RTM simulations (performed with the MODTRAN5v2 model [*Berk et al*., 2004]) that shows a mean bias of 0.6 W m^{-2} for a series of 30 carefully selected cases at a site where measured atmospheric profiles were available.

Similar methods (i.e., empirically based parameterizations and radiative transfer modeling) have been applied to derive surface LW↓ from satellite measurements. For example, *Gupta et al*. [1992] suggested some improvements to a previously developed parameterization [*Gupta*, 1989] that uses basically surface and air temperatures and water vapor burden measured from satellites (data from the International Satellite Cloud Climatology Project, ISCCP). With the improvements, mean difference with estimations from a detailed RTM was reduced to 1.7 ± 6.3 W m^{-2}. Later on, *Zhou and Cess* [2001] used an RTM to derive an algorithm to estimate LW↓. The algorithm used surface-emitted upward longwave radiation and precipitable water vapor (both measured from satellite) as main variables; under cloudy conditions, they found that the liquid water path is an adequate surrogate for cloud base height, in particular under partly cloudy skies. Subsequently, in order to extend the algorithm to high-altitude sites (such as Tibet) and cold climates, *Zhou et al*. [2007] added new variables such as the cloud fraction and the ice water path, which are available from the CERES products. When comparing with surface measurements at a number of sites across the world, they found an overall agreement of 1.2 ± 23.6 W m^{-2}.

The present study assesses the surface downward longwave fluxes estimated by using a one-dimensional radiative transfer model for overcast sky conditions and also by some parameterizations, in comparison with pyrgeometer measurements. The radiative transfer calculations are performed with the Santa Barbara discrete ordinates radiative transfer (DISORT) model (SBDART [*Ricchiazzi et al*., 1998]), while the parameterization suggested by *Konzelmann et al*. [1994] is tested. Special attention is devoted to describe the cloud radiative effect depending on the cloud base height (CBH) and to quantify the importance of including information on the CBH when estimating LW↓. Section 2 describes the characteristics of the instruments used in this study and the data set, including the selection of overcast cases. Section 3 introduces the RTM used, and section 4 describes a sensitivity study (based on both measurements and modeling) performed in order to confirm whether the CBH is the main variable driving the longwave radiation at the surface. Section 5 presents how estimations obtained with different inputs (in particular, regarding CBH) in both the RTM and the parameterization compare with measurements, explains the behavior of CRE depending on CBH and atmospheric conditions, and shows an extension of the study to different climates. Section 6 summarizes the main findings of the study.

2. Observational Data and Case Selection

Main data used in this study are taken from the radiometric and meteorological station (41°58′N, 2°50′E, 110 m above sea level) of the Physics Department of the University of Girona (Spain). Since this is the same station described in a previous work [*Viúdez-Mora et al*., 2009] here, only the most important aspects concerning the present study are highlighted. All data used (LW↓, surface air temperature and humidity, and CBH measured by a ceilometer) were averaged at 10 min intervals, regardless of their original sampling intervals.

2.1. Pyrgeometer Measurements and Case Selection

LW↓ is measured with a Kipp & Zonen CG1 pyrgeometer mounted on a Sun tracker (model 2AP by Kipp & Zonen) equipped with a shadowing device. The CG1 pyrgeometer is sensitive to the spectral range from 4 μm to 45 μm and has a field of view of 150°. The calibration factor, however, produces the LW↓ coming from the whole sky hemisphere and for the whole infrared range (2–100 μm). The "Kipp & Zonen CG1/CG2 Instruction Manual" indicates an "estimated accuracy of measurement" of ±10%, which is a very high

estimate, whereas the calibration certificate reports an uncertainty of about 7% for the calibration constant. This corresponds to the uncertainty in the net radiation term of the pyrgeometer equation (see Instruction Manual), mainly coming from the transfer in the comparison against the reference instruments. For overcast conditions (having a reduced net longwave flux with respect to clear-sky conditions), and accounting for the uncertainty in the measurement of the pyrgeometer's body temperature, a more realistic estimation of the measurement uncertainty for LW↓ would be lower than 3 W m^{-2}. Successive calibrations of the instrument performed at the Infrared Radiometry Section of the World Radiation Centre (WRC) that is part of the Physicalisch Meteorologisches Observatorium at Davos (PMOD/WRC) and at Kipp & Zonen facilities have given values very close to each other: 13.77 μV/W m^{-2} in 2007, 13.96 μV/W m^{-2} in 2009, and 14.42 μV/W m^{-2} in 2012.

The present study focuses on overcast conditions, so a number of cases corresponding to such conditions were selected from 3 years (2008–2010) of observations. To select these cases from the long databases, two automated methods for determining the cloud amount were applied: the so-called "automatic partial cloud amount detection algorithm" [*Dürr and Philipona*, 2004] and the method based on shortwave (solar) radiation measurements [*Long and Ackerman*, 2000] that has been further improved and nowadays also uses longwave measurements [*Long et al*., 2006b] to produce a whole day series of fractional sky cover estimation. When available, both methods have been applied independently; selected overcast cases have been chosen by imposing strict conditions (fractional sky cover greater than 98%) and subsequently removing rainy situations. With this selection, we consider that most cases must correspond to stratiform clouds. In addition, only cases for times when an atmospheric vertical profile was available (see below) were selected. A total of 82 situations were used: these cases are distributed along the four seasons (32 in winter, 11 in spring, 12 in summer, and 27 in autumn) and both in daytime (24 cases) and nighttime (58 cases).

2.2. Atmospheric Profiles

Due to the lack of information for the atmospheric profiles at the site and that the closest radiosoundings are 90 km southward (Barcelona) with remarkably different local conditions (Barcelona is on the Mediterranean coast so strongly influenced by local winds as sea breeze), all profiles corresponding to the 82 analyzed cases were obtained from the European Centre for Medium-Range Weather Forecasts (ECMWF) model, which produces analysis outputs every 6 h. Specifically, profiles were obtained by interpolation from the 2.5° × 2.5° original grid into a 1 km × 1 km mesh. Then we considered the profile generated for the cell where the measurement site is placed. An interpolation module integrated in the meso-NH model [*Lafore et al*., 1998] was used. Meso-NH is a nonhydrostatic mesoscale atmospheric model of the French research community, which is used in large variety of configurations. It can be applied to scales ranging from large (synoptic) to small (large eddies) [*Cuxart et al*., 2007].

2.3. Cloud Base Height Determination

Cloud conditions over the station can be directly determined with the help of a sky camera [*Long et al*., 2006a; *Calbó and Sabburg*, 2008] and a Vaisala CL-31 ceilometer. The ceilometer, which is in continuous operation, obtains backscattering profiles ranging up to 7500 m and delivers (by means of the algorithm provided by Vaisala) up to three cloud base heights with high time (12 s) and high vertical (10 m) resolution [*Costa-Surós et al*., 2013].

The height of the lower cloud layer can also be estimated from the atmospheric profiles, as an alternative method to the direct measurements provided by the ceilometer. This may be useful for a site where CBH measurements are unavailable. Various methods appear in the literature [*Poore et al*., 1995; *Wang and Rossow*, 1995; *Chernykh and Eskridge*, 1996]; we have selected the method proposed by *Zhang et al*. [2010] with the improvements suggested by *Costa-Surós et al*. [2014].

The method is summarized next. As a first step, the relative humidity (RH) with respect to liquid water is converted to RH with respect to ice when the temperature is below 0°C. Then, moist layers are identified by applying some conditions, which are related to a minimum RH threshold (min-RH) and to a minimum thickness (400 m). Note that the original method applies this latter condition only to moist layers with bases lower than 120 m; *Costa-Surós et al*. [2014] extended it to the whole atmospheric profile. Subsequently, moist layers are defined as cloud layers through some additional steps: (a) if the maximum RH within the layer

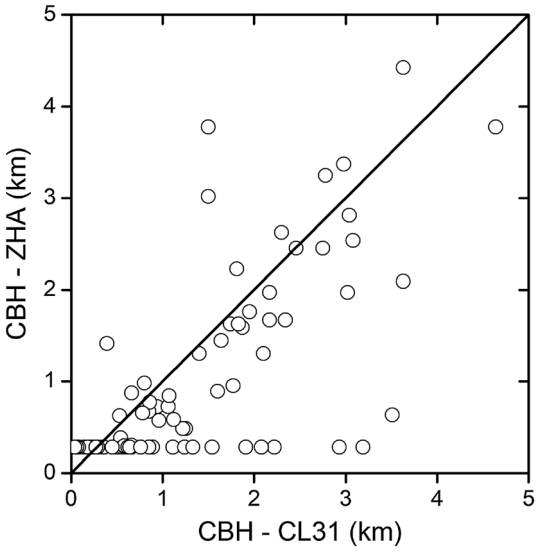

Figure 1. Comparison of cloud base height as derived from the vertical profile (CBH-ZHA) against the cloud base height from ceilometer measurements (CBH-CL31). The diagonal is the line of the perfect agreement. Two outliers (CBH-ZHA ~ 9 km) are not shown.

is greater than the corresponding maximum RH threshold (max-RH) for the base of this moist layer, (b) the base of cloud layers is set at least at 280 m above ground level, and (c) two contiguous layers are considered as a single-layer cloud if the distance between these two layers is less than 300 m or the minimum RH within this distance is greater than the corresponding inter-RH threshold value. Note that instead of single-humidity thresholds to define a cloud as in earlier works [*Wang and Rossow*, 1995; *Poore et al*., 1995], this method is based on altitude-dependent thresholds, which vary between 70% and 95% depending on the specific threshold (min-RH, inter-RH, and max-RH) and on the altitude (greater values of humidity thresholds correspond to lower atmospheric layers) [*Zhang et al*., 2010].

Therefore, two values of the CBH will be used when testing the RTM and the parameterization: CBH-CL31 will denote cloud base heights from ceilometer measurements; CBH-ZHA will denote estimations from applying *Zhang et al*. [2010]–*Costa-Surós et al*. [2014] method on the ECMWF derived vertical profiles of temperature and humidity.

Figure 1 shows the CBH estimated from the vertical profile (CBH-ZHA) against the CBH from ceilometer measurements (CBH-CL31). The agreement between them is fair, although it is obvious that CBH-ZHA has some deficiencies. First, there are a number of cases when CBH-ZHA takes the minimum value (0.28 km) while the measurements indicate that clouds are quite higher. This is due to the fact that the relative humidity in the first level of the atmospheric profile is higher than the required thresholds for a layer to be considered as a cloud. Second, there are two cases (not shown in Figure 3) when the opposite occurs: CBH-ZHA sets a cloud much higher (around 9 km) than the observed CBH. Finally, among the 82 cases, there are four cases for which the CBH-ZHA method does not detect any cloud since the relative humidity in the ECMWF-derived profile does not reach the specified thresholds at any level. These cases were not included in the comparison when using the CBH-ZHA data set. Nevertheless, CBH-ZHA captures, in general, the behavior of the cloud base height; so most values are arranged around the line of agreement. Note also that this analysis is not a proper assessment of the *Zhang et al*. [2010]–*Costa-Surós et al*. [2014] method, since the method is applied to synthetic profiles; for a detailed validation using in situ profiles, we refer the reader to the original references.

3. Radiative Transfer Model Configuration

As stated above, we have used SBDART [*Ricchiazzi et al*., 1998] for the estimations of LW↓ at the terrestrial surface. This model uses a discrete ordinate radiative transfer (DISORT) module [*Liou*, 1973; *Stamnes et al*., 1988] to solve the radiative transfer equation for a vertically inhomogeneous plane-parallel atmosphere. The configuration of the model is very similar to that used by *Viúdez-Mora et al*. [2009]; only the aspects that are different and relevant for the present study are detailed next. For all simulations, we have considered the atmosphere divided in 65 layers, with a resolution of 100 m up to 2 km, and then progressively decreasing with altitude. The uppermost layer is 15 km thick, between 85 km and the top of the atmosphere set at 100 km. The underlying terrestrial surface is assumed as a blackbody (the default option in the model). Ozone column was fixed to the values of the typical midlatitude summer (MLS) or midlatitude winter (MLW) atmospheres (324 and 403 Dobson unit (DU), respectively), and CO_2 concentration was fixed to the default

value of SBDART (360 ppm). Aerosols were introduced as rural, according to the nature of the site where the LW↓ measurements were taken. Aerosol optical depth was fixed to 0.1 at 550 nm (solar band).

The SBDART model presents some limitations, mainly its spectroscopy for gases, that is based on the Low Resolution Transmission model (LOWTRAN). Other, more accurate, state-of-the-art line-by-line (LBL) treatments may have overcome it. *Ricchiazzi et al*. [1998] stated that SBDART is not the best tool to make calculations in the longwave range, based on the comparison against atmospheric emitted radiance interferometer (AERI) measurements for a dry, cold, and clean atmosphere. These limitations have been reported by *Wacker et al*. [2009], who found, for cloudless night cases, that using LOWTRAN spectroscopy in radiative transfer calculations of the longwave broadband leads to an underestimation of about 6 W m^{-2}. However, when the atmospheric window is full (due to cloud emission) and the longwave radiation matches that of a blackbody, the spectroscopic resolution is no longer as important. Therefore, the use of SBDART should not be a handicap when assessing the effect of the CBH on LW↓ estimations (under overcast conditions) with reduced atmospheric information. Thus, taking into account the initial data sets available to initiate our tests (profiles calculated from a meteorological model and surface measurements of temperature and humidity) and the pyrgeometer measurement uncertainties, we considered the use of SBDART as a suitable option between the simple parameterizations and more rigorous treatments (as MODTRAN5 or state-of-the-art LBL models) when calculating downward longwave irradiance.

When estimating CRE, the use of LOWTRAN spectroscopy could introduce some bias through the calculation of the cloudless irradiance, which is subtracted from the calculated irradiance for the cloudy state. For the data set obtained at Girona, total precipitable water (TPW, derived from the atmospheric profiles) ranges from 0.8 to 4.2 cm, only four cases having values below 1 cm. Thus, the atmosphere cannot be considered dry for the considered data set, so it is expected that the mean bias introduced when calculating cloudless longwave irradiance should be lower than those 6 W m^{-2}. In fact, *Viúdez-Mora et al*. [2009] found, for cloudless conditions at Girona, very good agreement between SBDART and pyrgeometer measurements for cloudless skies, showing mean deviations between −0.7 and 1.8 W m^{-2} (the exact mean deviation depending on the origin of the atmospheric profile used), which are similar to or below the instrumental uncertainty. In summary, we only expect a small overestimation of CRE (a few W m^{-2}) when the atmospheric profile used to compute the cloudless reference shows remarkably cold and dry conditions.

Clouds can be introduced in the simulations as cloud layers at the calculation levels. Cloud properties such as the base height, thickness, cloud fraction, liquid/frozen water path, or cloud optical depth at 550 nm, and effective radius for the droplet or ice particle size distribution can be conveniently given by the user or alternatively left by default. In this work only one cloud layer has been introduced, and the cloud fraction has been fixed to 1, corresponding to overcast sky, both in the sensitivity analysis and in the tests. Cloud thickness has not been specified; thus, the model assigns the given whole liquid path or cloud optical depth to a single layer, according to the CBH. Finally, all simulations have been performed considering liquid cloud layers.

Note that the CBH that is actually introduced into the RTM (regardless of the method used to determine it) depends on the layers used when gridding the atmosphere. Therefore, there is some error associated to CBH due to the grid resolution, although this error is quite low in our study since the atmospheric layers are 100 m thick up to 2 km and less than 300 m thick in the studied CBH-CL31 range. Based on the results of the sensitivity analysis (see below), 100 m of error in the CBH assignation may result in a maximum error of 1.5 W m^{-2} in LW↓. Thus, the uncertainty associated to this problem, which is, in general, more relevant for lower level clouds [*Fung et al*., 1984], is reduced in our case because of the use of such a high vertical resolution in the lower layers of the atmosphere.

4. Sensitivity Analysis

For cloudless skies, the temperature and humidity profiles (especially at the lower atmospheric layers [*Ruckstuh et al*., 2007]) are the most important factors determining LW↓ [*Viúdez-Mora et al*., 2009] and therefore must obviously be taken into account, including the large diurnal and annual variability, when performing RTM LW↓ simulations [e.g., *Held and Soden*, 2000; *Dai et al*., 2002]. Specifically, *Viúdez-Mora et al*. [2009] showed that the sensitivity of LW↓ to changes in the temperature and humidity in the whole profiles is about 4 W m^{-2} K^{-1} and 0.65 W m^{-2} per percent change of water content, respectively.

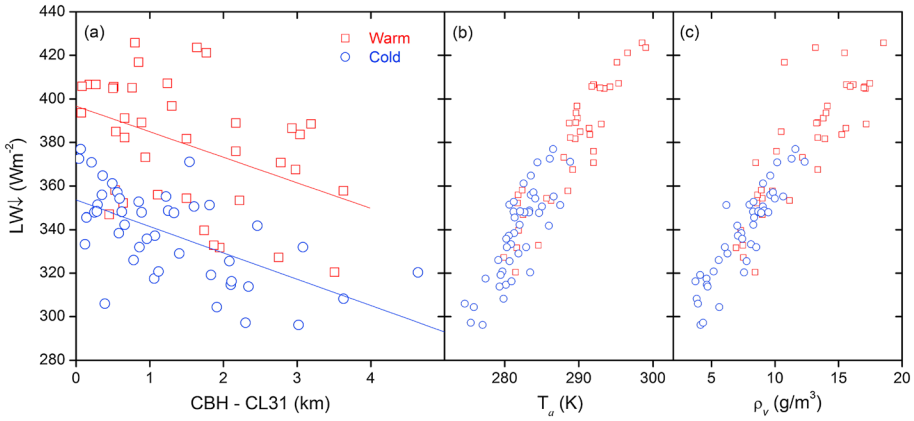

Figure 2. Downward longwave irradiance from pyrgeometer measurements against (a) cloud base height measured with the ceilometer, (b) screen-level temperature, and (c) screen-level water vapor content. All values are 10 min averages. Lines in Figure 2a correspond to the linear regression for each subset of points (warm and cold seasons).

For overcast skies, downward thermal radiation at the surface is mainly coming from the air between the surface and the cloud base, but the contribution of cloud emission within the atmospheric window may also be significant, so we must expect that besides the air conditions, the following cloud characteristics be of relevance: the liquid water path (LWP), the cloud droplet effective radius (R_{eff}), and the cloud base height (CBH).

With the available observations, we can perform a first analysis of the behavior of longwave radiation (LW↓ as measured by the pyrgeometer) against cloud height (CBH-CL31). Figure 2a shows this behavior, distinguishing the cases between those from the warm half of the year (climatic mean screen-level temperature higher than 15°C, May to October, 38 cases) and those from the cold half of the year (temperature lower than 15°C, November to April, 44 cases). Note that CBH of the selected cases is between 0 and 5 km, most cases (61) having CBH $<$ 2 km; the mean (and standard deviation) of CBH for the whole set of data is 1.4 ± 1.0 km (1.5 ± 1.0 km for the warm period and 1.3 ± 1.0 km for the cold period). Looking at all data, there is a large dispersion of points, so the effect of the CBH is not totally evident. However, observing separately each subset of data, a clear tendency of decreasing LW↓ with increasing CBH is shown in the figure. This tendency may be evaluated, as a first approximation, to be about -12 W m^{-2}/km, both for the "warm" points and the "cold" points. There is dispersion remaining in each subset: this dispersion comes from the fact that the represented cases correspond to different specific meteorological situations (so different temperature and humidity vertical profiles and different cloud characteristics).

A multiple linear analysis has been performed to have a simple assessment of the role of the main variables (temperature, humidity, and cloud base height) on LW↓ behavior. Thus, we have used LW↓ and CBH-CL31 measurements along with the screen-level air temperature (T_a) and absolute humidity (ρ_v) that are measured at the same station. Figures 2b and 2c show the strong dependence of LW↓ on T_a and ρ_v, respectively (in fact, T_a and ρ_v are highly correlated). For the multiple linear analysis, the four variables have been z standardized (i.e., transformed to 0 mean and 1 standard deviation). The correlation coefficients between LW↓ and T_a, ρ_v, and CBH are 0.93, 0.92, and -0.31, respectively. However, since T_a and ρ_v are also very much correlated ($r = 0.88$), CBH becomes the second most important variable (after T_a) to explain LW↓ variance: if T_a is used alone, the explained variance (r^2) of LW↓ is 0.87; when adding CBH, this increases to 0.95, while the subsequent addition of ρ_v has a minor effect ($r^2 = 0.97$). The linear model with the three independent standardized variables is LW↓ $= 0.69\, T_a + 0.26\, \rho_v - 0.24$ CBH. So it is clear that atmospheric temperature is the main factor to take into account when LW↓ is to be estimated; the cloud base height and the water vapor content have a similar weight, but the latter is highly correlated with temperature, so actually, its importance as estimator is reduced.

Moreover, modeling has been used to assess the sensitivity of LW↓ and CRE on cloud parameters. Here, besides the above explained conditions regarding model configuration, aerosols, CO_2 concentration, etc., we have considered some default conditions in SBDART to define a reference for the sensitivity simulations. For

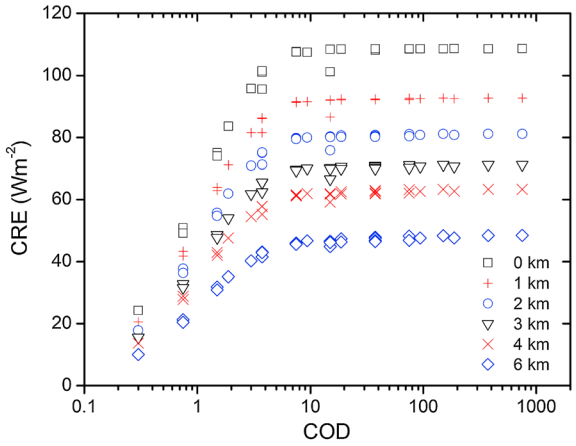

Figure 3. Dependence of the longwave cloud radiative effect (CRE) at the surface on the cloud optical depth (COD) for different cloud base heights. Note that for some values of COD and CBH, different values of CRE are obtained; this is due to the fact that different combinations of LWP and R_{eff} can produce (through equation (4)) the same values of COD.

example, the standard atmosphere US62, having a total ozone column of 349 DU, was chosen. Under these conditions and for cloudless sky, LW↓ was calculated to be 279.9 W m^{-2}, which is used as the reference value for the following sensitivity simulations.

Changing the parameters describing clouds in the model, we analyzed their effect on the simulated LW↓. Specifically, R_{eff} was varied within the 2–100 μm range, LWP was taken between 20 and 1000 g m^{-2}, and the CBH was considered from 0 to 6 km, representing low, middle, and high clouds (CBH = 0 means a cloud touching the ground, i.e., foggy conditions). The combination of LWP/R_{eff}/CBH values gives a total of 150 cases corresponding to cloudy conditions for the sensitivity analysis.

The RTM calculates LW↓, but here the analyzed variable is the cloud radiative effect at the surface, which is calculated as the difference between the irradiance when clouds are present and the irradiance for the reference cloudless sky case, i.e., with the same atmospheric profile and characteristics but without any cloud layer. On the other hand, despite introducing the liquid water path and the effective radius of droplets size distribution, the main property selected to show the radiative effect of clouds was the cloud optical depth (COD) at 550 nm (the center of the visible band), which combines these two properties with the scattering efficiency (Q), which is assumed to be two (in the shortwave visible band), in this way:

$$\mathrm{COD} = \frac{3Q\,\mathrm{LWP}}{4\rho R_{eff}}, \tag{4}$$

being ρ the water density. With the ranges of LWP and R_{eff} considered here, the range of COD extends from 0.3 to 750. Note that the COD as computed here corresponds to the optical depth in the visible wavelengths, but it is useful to summarize the cloud characteristics even when studying, as here, the interaction of clouds with longwave radiation.

The results of these calculations are shown in Figure 3. As expected, CRE at the surface decreases when CBH increases. This is easily explained because the clouds closer to the surface are usually warmer than higher clouds, so enhancing its IR emission. Note that for some values of COD and CBH, Figure 3 shows slightly different values of CRE, due to the fact that different combinations of LWP and R_{eff}, which are the actual properties that directly affect absorption and emission of radiation, can give (through equation (4)) the same values of COD. Differences are almost imperceptible, except for the lowest value of LWP. For example, the value of COD = 15 in Figure 3 was obtained from three combinations of R_{eff} and LWP: 2 and 20, 20 and 200, and 100 and 1000, producing, for CBH = 1 km, a CRE of 86.6, 92.2, and 92.0 W m^{-2}, respectively. The reason for these differences, as above noted, is because the dependence of the longwave cloud optical depth on LWP and R_{eff} is slightly different than in the visible. Indeed, equation (4) assumes that the scattering efficiency Q is equal to two, which is valid for wavelengths much shorter than R_{eff}. Within the thermal infrared band, however, wavelength and size of cloud droplets are of the same order of magnitude, so the assumption of $Q = 2$ may not be valid.

From Figure 3, we can infer that the cloud base height (to which the emission temperature is linked) is the main variable determining LW↓ for a given atmospheric vertical profile, whereas cloud optical depth is relevant only for thin clouds (COD < 10). From this sensitivity study, we can see that for thick clouds with CBH = 1 km, CRE is about 92 W m^{-2} while CRE is about 47 W m^{-2} for the highest clouds considered (CBH = 6 km). The values of CRE for much thinner clouds are notably lower: for COD = 1, CRE is approximately

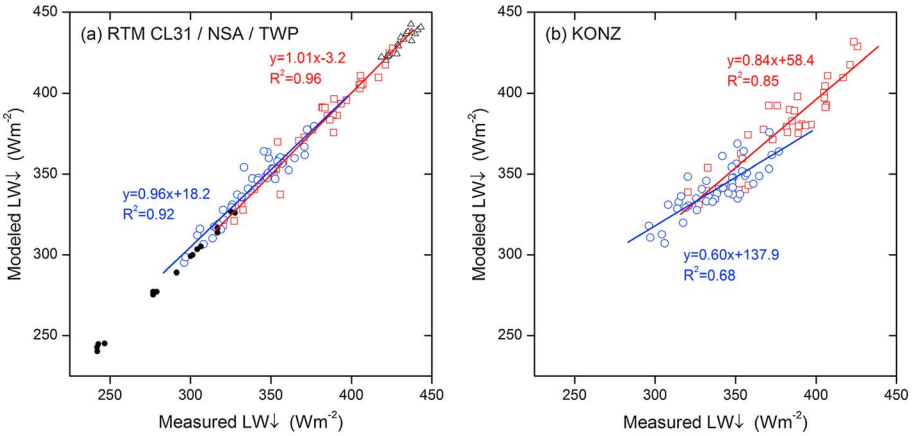

Figure 4. Comparison between calculated and measured LW↓, during overcast conditions, (a) for the RTM results when using CBH measured by ceilometer and (b) for the [*Konzelmann et al.*, 1994] parameterization results. See text for definition of tests. Warm season data (red) and cold season data (blue) at Girona are distinguished in the plots. The linear regression lines are given for both subsets of data. In Figure 4a, black circles correspond to NSA cases (subarctic climate) and open black triangles correspond to TWP (tropical climate).

50% lower. In addition, from the sensitivity study, one can easily retrieve that the CRE decreases with CBH at a ratio between 16 W m^{-2}/km at the lowest levels and 8 W m^{-2}/km at the highest levels (6 km) for optically thick clouds. Therefore, this analysis confirms the importance of the CBH (and COD), besides the temperature and humidity profiles, when studying LW↓ at the surface under cloudy conditions.

5. Results and Discussion

5.1. Effect of CBH on the Agreement Between Modeled and Measured LW↓

Several modeling tests were performed. These consist in using available relevant information about the atmospheric conditions as input information for the radiative transfer model when estimating LW↓ and then testing the agreement between model results and measurements. As concluded in the sensitivity study, the most important factors determining LW↓ at the surface for overcast skies are the CBH and the cloud optical depth, besides the temperature and humidity vertical profile. At our station in Girona, CBH is directly measured by the ceilometer, or it can be estimated from the atmospheric profile. Both values CBH-CL31 and CBH-ZHA were used when testing the RTM. In a third experiment, CBH was fixed to 2 km (CBH-FIX) to check the case that neither measurements nor estimations of CBH were available. This latter test aims at setting a reference for the modeling-measurement differences, since it should represent the worst case.

In Girona, there is no direct information to estimate microphysical cloud properties. To overcome this lack of information, some fixed values were used for the RTM calculations. These fixed values were taken from the experimental study of *Stephens* [1978]. Specifically, that study tried to characterize some cloud properties such as the droplet (or ice crystals) effective radius and the liquid water path. According to this reference, and given that in most cases our data set presents stratiform clouds, the cloud parameters were fixed to the values suggested for this kind of clouds, 7.5 μm and 1000 gm^{-2}, respectively, for effective radius and liquid water path. These assumptions produce an optical depth of 200 (equation (4)), which corresponds to very thick, and consequently, opaque clouds.

The comparison of the model results against the measurements, for the three sets of tests above described, is presented next. There is a general agreement between RTM estimations of LW↓ and the corresponding observations. Figure 4a shows the comparison for the CBH-CL31 case, including regression parameters between RTM calculations and measurements. This is the best case based on the coefficients of the regression; for the ZHA and FIX cases (not shown), both the slope and the intercept of the regression line are successively worse, and the determination coefficient lower. Note that results for other sites corresponding to subarctic and tropical climates that are treated in section 5.4 are also shown.

Table 1. MD and SD of Differences Between Modeling Estimations and Measurements[a]

	Annual			Warm			Cold		
Tests	N	MD	SD	N	MD	SD	N	MD	SD
RTM-CL31	82	1.6	6.2	38	−0.1	5.9	44	3.1	6.1
RTM-ZHA	76	4.3	7.0	35	2.5	7.4	41	6.0	6.1
RTM-FIX	82	−2.5	9.4	38	−2.9	9.1	44	−2.2	9.8
KONZ	82	1.1	11.6	38	−0.7	11.1	44	2.6	11.9
KONZ-CL31	82	−0.1	7.3	38	−3.0	7.6	44	2.4	6.1
KONZ-ZHA	76	3.1	9.4	35	0.3	10.4	41	5.6	7.5
NSA	16	−0.9	1.4	8	−1.0	1.3	8	−0.8	1.6
TWP	18	0.2	2.9						

[a]Units are W m^{-2}. N is the number of cases included in each test and comparison. The four cases when ZHA method does not detect any cloud and the two outliers are removed from the MD and SD calculations in RTM-ZHA and KONZ-ZHA tests. RTM means test based on the SBDART radiative transfer model, and KONZ means test based on *Konzelmann et al.* [1994] parameterization; NSA stands for the subarctic site, and TWP refers to the tropical site. See text for further details on tests.

These results are confirmed by the metrics of agreement provided in Table 1: the bias or mean deviation (MD), which is an average of the model minus the measured values, and the standard deviation of the differences (SD), as a measure of dispersion. Indeed, the best indices correspond to the CL31 test, i.e., when the observed CBH is used. In this test, dispersion of residuals is very low (6.2 W m^{-2}) and bias is very low too (1.6 W m^{-2}). The good behavior of this test is reproduced as well if we analyze the warm season and the cold season data separately. Tests built upon the ZHA estimations of CBH are clearly worse. Even if we remove from the analysis the two outliers (corresponding to two very large overestimation of CBH-ZHA for two cold season cases), bias is larger (4.3 W m^{-2}), and dispersion is also increased (7.0 W m^{-2}). This worsening is very similar in both seasons, although the cold season bias is remarkably higher. Possible deficiencies in the synthetic profile (in particular, too high humidity at the lower levels) may explain the poor results of ZHA method for CBH estimation and the general tendency toward overestimation that show the ZHA test results.

Finally, results for the reference case (FIX) are, as expected, even worse (dispersion 9.4 W m^{-2}), but the bias (−2.5 W m^{-2}) is similar to that of the other tests. This latter result would suggest that using a fixed CBH could lead to good enough results. However, this is not generalizable, because we have fixed here, by chance, the CBH to a value (2 km) very close to the mean CBH in the data set: that is, the reason for the low bias in the modeling results. If the difference between the fixed CBH and the average actual CBH would have been of 1 km, the modeled LW↓ would have had a bias of about ±10 W m^{-2} (based on the results of our sensitivity study). Note that the mean absolute bias (not shown in the table) of the FIX test (7.7 W m^{-2}) is quite greater than that of the CL31 test (4.6 W m^{-2}) therefore confirming that the latter is the best experiment.

Even in the best test (CL31) there are some particular cases when the difference between model estimation and measurement is quite remarkable. Specifically, there are six cases that lie outside the range of MD ± 2 × SD: four overestimations of 15.4, 15.6, 18.4, and 20.8 W m^{-2} (three of them corresponding to cold season cases) and two underestimations of −13.5 and −18.5 W m^{-2} both corresponding to warm season cases. The measured CBH for these six cases were 1.50, 0.25, 0.14, 0.12, 2.17, and 1.11 km, respectively (the three lowest clouds corresponding to the winter cases).

There are several potential causes that would explain these extreme differences (which may be also valid for other lower differences). On the one hand, there are the cloud characteristics. If the cloud was thinner than we have assumed in the model simulations, the RTM would overestimate the actual (measured) LW↓. Based on our sensitivity analysis (section 4), a thin cloud (optical depth equal to 4) produces about 5–10 W m^{-2} less irradiance as compared with a thick (optical depth greater than 10) cloud. Thus, the presence of a thin cloud or elevated fog in the winter cases, instead the assumed thick cloud, could explain the above mentioned large overestimations. In addition, the CBH measurement is performed by a ceilometer, which produces a pure vertical "pencil" view of the sky. This means that despite of the 10 min averaging, it may happen that the measured CBH is not representative of the whole cloud cover. Note that most extreme differences discussed here are at nighttime, so we cannot use the whole sky camera to confirm whether the cloud cover was homogeneous. For the only daytime case (which is the overestimation of 15.6 W m^{-2} that corresponds to

19 January 2010 at 12:00) camera images confirm a low, thick cloud, probably with fog patches below it. On the other hand, vertical profiles are not taken in situ but are produced from a gridded analysis provided by the ECMWF (section 2.2). Despite these profiles might be, in general, a good approximation, it may well happen that they fail to capture some detail of the actual profile (a surface layer inversion, for example) or that they are cooler and drier (or warmer and wetter) than the actual atmosphere. In this sense, note that the three largest overestimations correspond to winter time, so the profile could be warmer/wetter than the real profile, while the large underestimations correspond to summer time, so the profile could be cooler/drier.

To try to check this issue, we used the local surface measurements of temperature and humidity. For the 82 cases analyzed, the mean difference in temperature (first level of the ECMWF interpolated profile minus on-site measurement) is 0.0 ± 1.4 K, while the mean difference in water vapor content is -1.0 ± 1.1 g m^{-3}. There are some particular cases where the differences are larger, between -3.8 and +3.1 K and between -6.1 and 0.9 g m^{-3} for temperature and water vapor content, respectively. These differences may result in errors of up to 10 W m^{-2} in the estimated LW↓, based upon results of the sensitivity analysis in *Viúdez-Mora et al.* [2009], although the effect will be much lower in most cases. However, the six largest deviations of LW↓ estimations compared to measurements do not correspond to the largest differences in temperature/humidity at the surface, so the largest deviations remain mostly unexplained.

Our results may be compared with some previous works. For example, in a similar study, *Viúdez-Mora et al.* [2009] used the same RTM and the same site (so the same pyrgeometer for measurements) to explore the modeling of LW↓ for cloudless cases. In that study, the overall differences (model minus measurements, when using the same strategy for simulations, i.e., ECMWF-derived profiles) were found to be 0.4 ± 9.4 W m^{-2}. This means that the inclusion of clouds (with the CBH correctly measured by a ceilometer) tends to very slightly increase bias and to reduce dispersion. This is logical since for overcast skies the CBH plays an important role, while the temperature and humidity vertical profiles reduce their impact on results. On the other hand, *Wacker et al.* [2011] showed that for very well selected cases of one kind of low-level clouds (stratus nebulosus), the agreement between a RTM estimation and measurements of LW↓ may be as good as 0.6 ± 1.5 W m^{-2}. Note that this latter study analyzed only 30 cases, for only one season (fall) and with CBH varying only between 55 and 840 m, and used in situ-measured vertical profiles. Results from *Zhou et al.* [2007] show a similar MD (1.2 W m^{-2}) but a much larger dispersion (SD = 23.6 W m^{-2}); note, however, that these latter results correspond to a comparison for several sites in the world that include extreme climates (desert, high mountain, polar,…) and also include partly cloudy conditions.

5.2. Including CBH in Simple LW↓ Parameterizations

An alternative way to estimate LW↓ is by means of a simple parameterization based on ground-level measurements of temperature and humidity, as above commented (section 1). Several suitable parameterizations, intended for cloudy skies, were checked; results of only one of them [*Konzelmann et al.*, 1994], which produces quite good agreement with measurements (despite of being derived with Greenland data), are shown here and compared with results of the RTM computations. This parameterization can be expressed as follows:

$$\mathrm{LW}\downarrow = \mathrm{CMF}\ \ \mathrm{LW}_{\mathrm{cs}}\downarrow = \ \left[(1-n^p) + \varepsilon'_{\mathrm{oc}} n^p\right] \varepsilon_{\mathrm{atm}}(T_a, e)\sigma T_a^4 \tag{5}$$

where n is the cloud amount and p and $\varepsilon'_{\mathrm{oc}}$ (subindex oc means overcast) are parameters describing the effect of clouds that were adjusted to the data. For overcast conditions ($n = 1$) the parameterization becomes very simple:

$$\mathrm{LW}_{\mathrm{oc}}\downarrow = 0.952\sigma T_a^4 \tag{6}$$

Thus, Figure 4b shows the scatterplot of estimations from this formula versus measurements; the agreement is fair, but the coefficients of the regression are clearly worse than those from the RTM computations, in particular for the cold season cases. The statistical measurements of the agreement are shown in Table 1; the bias is quite low, but the standard deviation of the differences is the highest, so indicating the large dispersion of these estimations when compared with the measurements.

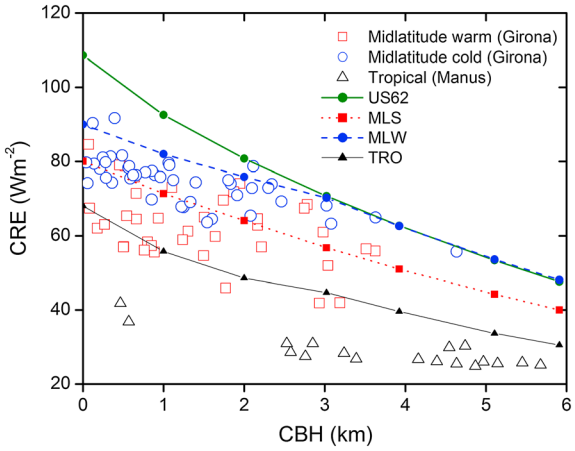

Figure 5. Cloud radiative effect against measured cloud base height. Warm season (red squares), cold season (blue circles) values corresponding to midlatitude cases (Girona), and tropical cases (Manus, black triangles) are distinguished. The CRE as derived from the sensitivity analysis is also plotted (green). The CRE as derived by adding a cloud at different levels within atmospheres representative of conditions for "midlatitude summer," "midlatitude winter," and "tropical" is also represented.

The parameterization does not take into account the cloud base height, which we know that it is an important factor describing LW↓ under overcast skies. Therefore, we plotted the ratio between estimations and measurements against the measured CBH and fitted a correction for the parameterization:

$$\begin{aligned} LW\downarrow &= LW_{oc}\downarrow f(CBH) \\ &= 0.952\sigma T_a^4 (1.031 - 0.025\ \ CBH) \end{aligned} \tag{7}$$

where CBH is in kilometers. With this modification and using the same measurements of CBH by the ceilometer, the agreement with measured longwave irradiance improves notably (see Table 1): dispersion is at the same level as the RTM-ZHA test, and bias is very low (note, however, that this comes from the fact that the bias is calculated on the same set of data used to derive the modification factor accounting for the CBH effect). Still, another test was performed: the use of the modified Konzelmann parameterization with the CBH as it is estimated by ZHA method applied to ECMWF interpolated profiles. As expected, results show a moderate dispersion of the differences (9.4 W m^{-2}) with a slight positive bias produced by the underestimation of CBH from the ZHA method.

5.3. Cloud Radiative Effect Dependence on CBH

The cloud radiative effect (CRE) at the surface can also be evaluated for the set of analyzed cases. Specifically, CRE is calculated as the difference between the results of the RTM for the actual overcast conditions (with CBH-CL31) and the corresponding estimations (from the same RTM) of LW↓ for a cloudless sky. For this latter calculation, the same atmospheric profiles from ECMWF were used but without introducing the cloud layer into the cloud properties file. Note that despite of not considering the cloud, the atmospheric profile is the same, so it usually contains high water vapor in the layers between the ground and the cloud (and within the cloud, of course). Results (CRE versus CBH) are presented in Figure 5, along with the CRE for thick clouds derived from the sensitivity study. The main tendency of CRE decreasing with CBH is apparent in the plot. The seasonal behavior of CRE is also quite evident: in general, CRE for the cold season is greater than CRE for the warm season. We also find a noticeable case-to-case (i.e., due to the particular meteorological conditions represented in the vertical profile) variability. Thus, CRE is about 80 W m^{-2} for low clouds (0–1 km) in the cold season and decreases to around 60 W m^{-2} for medium clouds (3–5 km) in this same season; in the warm half of the year, CRE is about 65 W m^{-2} for low clouds (0–1 km) and even less than 50 W m^{-2} for medium clouds (3–4 km). The decreasing rates of CRE with CBH are −5 and −4 W m^{-2}/km for the cold season and the warm season, respectively. Note also the greater dispersion of the points representing the warm period. The approximate value given for the cold season and low clouds is identical to the value found by *Wacker et al.* [2011], 80.0 ± 2.8 W m^{-2}, for a set of 30 cases of very low clouds (lower than 850 m) during the fall season in Switzerland.

Also in Figure 5, it is evident that CRE calculated here for real cases is lower than those estimated from the sensitivity study (section 4), for which the US62 atmosphere was used. The use of a fixed cloud optical depth cannot explain these differences: even if we assume a very thin cloud (COD ~ 3), CRE derived from the sensitivity study is higher than most values shown in Figure 5. We know, in addition, that the assumption of thick clouds is quite correct, since the estimations of LW↓ agree quite well with measurements as above commented. The discrepancy has, however, an explanation: in the sensitivity analysis, we had prescribed a cloud within an average (standard) atmospheric profile that reflects cloud-free conditions (that is with

relative humidity of about 45–50% in the lower troposphere); contrarily, when modeling real cases, profiles reflect conditions (temperature and humidity) corresponding to the presence of clouds, even if the cloud itself is "switched off" in the simulation performed to compute the "cloudless" case in order to calculate the CRE. In other words, the CRE values from the sensitivity analysis are higher and may be considered as a maximum value because the effect of the atmosphere between the cloud and the ground (and in particular in the lowest levels of the atmosphere) is reduced in comparison with the real wetter atmospheres usually found when clouds are present. In fact, if we repeat part of the sensitivity analysis by using other standard atmospheres representing summer and winter conditions ("midlatitude summer" and "midlatitude winter" atmospheres provided by the RTM), the obtained CRE as function of CBH is much more similar (although usually higher) to the values found for the real cases or our database (see Figure 5). Another potential source of uncertainty in our estimation of CRE is the use of a low-resolution spectroscopy in the RTM which could underestimate the downward longwave irradiance by a few W m^{-2} for the cloudless conditions (in particular for cold and dry conditions, as above explained), leading to a slight overestimation of the CRE.

5.4. Extension to Other Climates

Results presented up to this point correspond to atmospheric conditions at Girona, which may be representative of midlatitude climates. Note, for example, that the range of surface temperatures for the considered cases is 1.5–25.9°C, while the TPW is in the range 0.8–4.2 cm. It is obvious, however, that conditions corresponding to some climates are away from these ranges, so validity in other climates of some of the above methods and results are checked in this section. Specifically, measurements of LW↓ by a pyrgeometer, observations of CBH by a ceilometer, and atmospheric profiles obtained by radiosoundings at Barrow, Alaska (NSA), and Manus, Papua New Guinea (TWP), have been used. These two sites represent subarctic and tropical climates, respectively; both stations belong to the Atmospheric Radiation Measurement program (ARM) [*Ackerman and Stokes*, 2003], so the quality of the measurements is quite assured. At these two sites, a limited number of overcast cases (which, however, extend across the year and correspond to different hours within the day) have been selected. The ranges of surface temperature and TPW are 24.0–28.3°C and 5.3–6.5 cm and −22.4–4.2°C and 0.5–1.6 cm for TWP and NSA, respectively. The radiative transfer model has been applied with the same configuration as for Girona cases; the only difference is the use of actual vertical profiles, which have been extended up to 100 km by using the corresponding standard atmosphere ("subarctic winter," "subarctic summer," or "tropical").

Modeling results are presented in Figure 4 against measured LW↓, while the main statistical indexes of the model-measurement comparison are shown in Table 1. It is evident that the agreement between measurements and RTM estimations is very good, in particular for the NSA cases. Actually, both MD and SD are lower than the corresponding values obtained for Girona. The use of actual profiles of temperature and humidity in NSA and TWP instead of the synthetic profiles (in Girona) explains this better agreement.

On the other hand, Figure 5 shows the behavior of the cloud radiative effect in the tropical climate. Like in the case of Girona, CRE derived from using the tropical standard atmosphere is also plotted. Again, the latter values must be considered as maximum values because of the reasons already commented (see section 5.3). CRE for the tropical site cases is between 25 and 40 W m^{-2}, with a clear role of CBH (CRE decreases approximately 2.5 W m^{-2}/km of CBH). These values are clearly lower than those found for Girona, which is a consequence of the warmer and wetter atmosphere of the tropical climate. Thus, the effect of a cloud is lower when its longwave emission is added to an already very humid air (that is, with the atmospheric window closer to saturation). Moreover, the values found for the real cases are markedly lower than those derived from the standard atmosphere. Again, this is mainly due to the fact that the real profiles are notably wetter (TPW = 5.3–6.5 cm) than that of the standard tropical atmosphere (TPW = 4.2 cm).

At the subarctic site, we have found CRE values of around 60–80 W m^{-2}. Values are not shown since the dependence on CBH is hardly visible, given that most cases have very low clouds (CBH $<$ 300 m). Therefore, in our data set, the range of CRE values is mainly explained by the differences in temperature and humidity profiles. Regarding the standard atmospheres, CRE values range from 90 W m^{-2} to 50 W m^{-2} in summer for very low clouds (CBH close to 0 km) and high clouds (CBH = 5 km), respectively. The variation of CRE with CBH for the winter subarctic standard atmosphere is not monotonous and presents a maximum (80 W m^{-2}) at about 1 km. This is due to the persistent temperature inversion that exists in this climate in winter, which makes that a cloud at such height has a warmer base (i.e., emits more longwave radiation) than a cloud at lower altitude.

6. Conclusions

We have performed a deep analysis of the behavior of the downward longwave (infrared) radiation that reaches the Earth surface under overcast conditions by using radiative transfer model simulations as a research tool. Results from the analyses point toward the double role of CBH on LW↓: first, CBH defines the temperature of the lowest cloud boundary (the cloud base), which through the Stefan-Boltzmann law drives the cloud emittance, and second, CBH somewhat discriminates between those atmospheric layers that will add their effect on LW↓ (i.e., layers between the cloud base and the ground) from those that will not have any effect (i.e., layers above the cloud). Very high atmospheric layers do not have any effect on LW↓ even under cloud-free skies, but under overcast conditions, infrared radiation emitted by the atmospheric layers above a cloud is totally absorbed by the cloud itself, at least for thick enough clouds (COD > 10).

Clouds always have a positive radiative effect on LW↓, that is, they always add radiation to that coming from a cloud-free atmosphere. Specifically, the cloud radiative effect is between 80 W m^{-2} for low-level clouds in cold atmospheric conditions (cold meaning late fall or winter conditions at a midlatitude—Mediterranean climate—site) and less than 50 W m^{-2} for higher clouds in the warm season. The decreasing rates of CRE with CBH are -5 and -4 W m^{-2}/km for the cold and the warm seasons, respectively. These values have been calculated from the RTM simulations of the real cases analyzed in this study. Nevertheless, an additional RTM-based sensitivity study performed by means of introducing an "artificial" cloud in a standard atmosphere, gives maximum values of CRE that are slightly higher, so confirming the previous results. For a tropical climate, the CRE is much lower (40–25 W m^{-2}), since in a very wet atmosphere the longwave emission from clouds adds less radiation to the already important water vapor emission. For a subarctic climate, we have found CRE, for very low clouds (CBH < 300 m), in the range of 60–80 W m^{-2}.

LW↓ for overcast skies can be quite correctly simulated by an RTM, even if it is relatively simple and based on a low-resolution spectroscopy (as the model used here, SBDART), and using as input synthetic profiles obtained through a physically sound interpolation of the gridded values of the ECMWF analysis. When the ceilometer measurements of CBH are introduced in the RTM, the model-measurement agreement is very good (1.6 ± 6.2 W m^{-2}), showing a bias clearly within the measurement uncertainty. If no CBH measurements are available, there are two options for the simulations (other than the mere visual estimation of the CBH, which is anyway limited to daylight periods), either using an estimation of the CBH by a suitable method based on the vertical profile of atmospheric temperature and humidity or using a fixed value of the CBH (which must be close to the average CBH for the site). When applied to our data set, results of these two options successively increase the dispersion of the model-measurement differences (up to 7.0 and 9.4 W m^{-2}, respectively). If actual radiosounding profiles are used as input in the RTM, along with ceilometer measurements of the CBH, the dispersion of the differences is greatly reduced (up to less than 3 W m^{-2}), as shown from the simulation of cases for two sites at tropical and subarctic climate.

As mentioned, the above results for Girona have been obtained for a site where no in situ radiosoundings were available. Since the vertical profile of temperature and humidity is a key factor conditioning LW↓, synthetic profiles were used. Despite this limitation, results of the present study show internal consistency and are also coherent with previous published results. In addition, they are potentially useful for applications where neither measured vertical profiles nor measured CBH are available. In this latter case, an alternative would be to use a simple parameterization based on ground-level meteorological measurements. This produces greater differences (SD = 11.6 W m^{-2}), which can be somewhat reduced if the parameterization is modified to include a factor depending on CBH (and CBH is measured or estimated).

In summary, this paper assesses the uncertainty that one may expect when estimating LW↓ under overcast conditions by different methods, with different complexity and needs of data. If only surface meteorological data are available, a first estimation may be performed with a parameterization (such as *Konzelmann et al.* [1994]), which, for overcast conditions, only needs ambient temperature. If more accuracy is needed, one may search for vertical atmospheric profiles (from a close location or from a gridded reanalysis, such as those provided by ECMWF) and use an RTM (e.g., SBDART) and fix an average CBH. From the same profiles, CBH may be estimated by means of a suitable method (such as *Zhang et al.* [2010]–*Costa-Surós et al.* [2014]). This estimation may be used in the modified parameterization suggested here or may be used as input in the RTM simulations. If measurements of CBH are available (usually from a ceilometer, which is a typical instrument in

an airport), the actual CBH may be input in the modified parameterization or, for best results, in the RTM computations. One should expect that dispersion of residuals would be reduced by a factor of 2 from the first estimation up to this latter option. If actual atmospheric profiles (either from radiosoundings or from aircrafts) are used, further reduction of residuals is expected.

The overall assessment presented here may be useful in models of surface energy balance in both natural and artificial surfaces (as ice sheet, glaciers, lakes, urban areas, …) or in the assessment of evapotranspiration (for forest, agricultural, or hydrological cycle studies). Usefulness extends to any application where an estimation of the downward longwave irradiance is needed (e.g., to calculate the energetic balance in buildings, greenhouses, pools, solar energy plants, snow melt in buildings, roads or ski slopes, in the forecasting of nocturnal frosts or fogs, etc.). If the application is in climate studies, it must be recalled that an error of 100 m in CBH may produce an error of up to 1.5 W m^{-2} in LW↓ (and in CRE). Provided that this error is not systematic, the overall uncertainty of a long-term data set would be lower. Therefore, the methods presented here could be used for defining the climatic values of LW↓ (and CRE) in a given region, although they may not be suitable for climate trend studies, since decadal trends can be of a similar magnitude as the commented errors.

Acknowledgments

This study has been partly financed by the Spanish Ministry of Science and Innovation (currently Ministry of Economy and Competitiveness) projects NUCLIEREX (CGL 2007-62664/CLI) and NUCLIERSOL (CGL 2010-18546). The European Centre for Medium-Range Weather Forecasts (ECMWF) is acknowledged for providing the meteorological analyses used in the present study. NSA and TWP data were obtained from the Atmospheric Radiation Measurement (ARM) Program sponsored by the U.S. Department of Energy, Office of Science, Office of Biological and Environmental Research, Climate and Environmental Sciences Division. We would like to thank M. Antonia Jiménez from the University of Illes Balears for helping us in preparing the atmospheric profiles from the ECMWF analysis. Data used to produce the results of this paper are available by request to the authors; please contact them at josep.calbo@udg.edu.

References

Ackerman, T. P., and G. Stokes (2003), The Atmospheric Radiation Measurement Program, *Phys. Today*, *56*, 38–45.

Ångström, A. (1915), *A Study of the Radiation of the Atmosphere Based Upon Observations of Thenocturnal Radiation During Expeditions to Algeria and to California*, *Smithsonian Misc. Collect.*, vol. 65, p. 159, Smithsonian Institution, Washington, D. C.

Arking, A. (1991), The radiative effects of clouds and their impact on climate, *Bull. Am. Meteorol. Soc.*, *71*(6), 795–813.

Berk, A., et al. (2004), MODTRAN5: A reformulated atmospheric band model with auxiliary species and practical multiple scattering options, *SPIE Conf. Ser.*, *5425*, 341–347, doi:10.1117/12.546782.

Boucher, O., et al. (2013), Clouds and aerosols, in *Climate Change 2013: The Physical Science Basis. Contribution of Working Group I to the Fifth Assessment Report of the Intergovernmental Panel on Climate Change*, edited by T. F. Stocker et al., pp. 571–658, Cambridge Univ. Press, Cambridge, U. K., and New York.

Bréon, F.-M., R. Frouin, and C. Gautier (1991), Downwelling longwave irradiance at the ocean surface: An assessment of in situ measurements and parameterizations, *J. Appl. Meteorol.*, *30*, 17–31.

Calbó, J., and J. Sabburg (2008), Feature extraction from whole-sky ground based images for cloud type recognition, *J. Atmos. Oceanic Technol.*, *25*, 3–14, doi:10.1175/2007JTECHA959.1.

Chen, T., W. B. Rossow, and Y. C. Zhang (2000), Radiative effects of cloud-type variations, *J. Clim.*, *13*, 264–286.

Chernykh, I. V., and R. E. Eskridge (1996), Determination of cloud amount and level from radiosonde soundings, *J. Appl. Meteorol.*, *35*, 1362–1369.

Chylek, P., and J. G. D. Wong (1998), Cloud radiative forcing ratio—An analytical model, *Tellus A*, *50*(3), 259–264.

Chylek, P., P. Damiano, and E. P. Shettle (1992), Infrared emittance of water clouds, *J. Atmos. Sci.*, *49*, 1459–1472.

Costa-Surós, M., J. Calbó, J. A. González, and J. Martin-Vide (2013), Behavior of cloud base height from ceilometer measurements, *Atmos. Res.*, *127*, 64–76, doi:10.1016/j.atmosres.2013.02.005.

Costa-Surós, M., J. Calbó, J. A. González, and C. N. Long (2014), Comparing the cloud vertical structure derived from several methods based on measured atmospheric profiles and active surface measurements, *Atmos. Meas. Tech.*, *7*, 2757–2773, doi:10.5194/amt-7-2757-2014.

Crawford, T. M., and C. E. Duchon (1999), An improved parameterization for estimates effective atmospheric emissivity for use in calculating day-time downward longwave radiation, *J. Appl. Meteorol.*, *38*, 474–480.

Cuxart, J., M. A. Jiménez, and D. Martínez (2007), Nocturnal meso-beta basin and katabatic flows on a midlatitude island, *Mon. Weather Rev.*, *135*, 918–932.

Dai, A., J. Wang, R. H. Ware, and T. Van Hove (2002), Diurnal variation in water vapor over North America and its implications for sampling errors in radiosonde humidity, *J. Geophys. Res.*, *107*(D10), 4090, doi:10.1029/2001JD000642.

Dürr, B., and R. Philipona (2004), Automatic cloud amount detection by surface longwave downward radiation measurements, *J. Geophys. Res.*, *109*, D05201, doi:10.1029/2003JD004182.

Fu, Q., and K. N. Liou (1993), Parameterization of the radiative properties of cirrus clouds, *J. Atmos. Sci.*, *50*, 2008–2025.

Fung, I. Y., D. E. Harrison, and A. A. Lacis (1984), On the variability of the net longwave radiation at the ocean surface, *Rev. Geophys. Space Phys.*, *22*, 177–193.

Gröbner, J., S. Wacker, L. Vuilleumier, and N. Kämpfer (2009), Effective atmospheric boundary layer temperature from longwave radiation measurements, *J. Geophys. Res.*, *114*, D19116, doi:10.1029/2009JD012274.

Gupta, S. K. (1989), A parameterization for longwave surface radiation from sun-synchronous satellite data, *J. Clim.*, *2*, 305–320.

Gupta, S. K., W. L. Darnell, and A. C. Wilber (1992), A parameterization for longwave surface radiation from satellite data: Recent improvements, *J. Appl. Meteorol.*, *31*, 1361–1367.

Held, I. M., and B. J. Soden (2000), Water vapor feedback and global warming, *Annu. Rev. Energy Environ.*, *25*, 441–475.

Iziomon, M. G., H. Mayer, and A. Matzarakis (2003), Downward atmospheric longwave irradiance under clear and cloudy skies: Measurement and parameterization, *J. Atmos. Sol. Terr. Phys.*, *65*(10), 1107–1116, doi:10.1016/j.jastp.2003.07.007.

Jacobs, J. D. (1978), Radiation climate of Broughton Island, in *Energy Budget Studies in Relation to Fast-Ice Breakup Processes in Davis Strait*, edited by R. G. Barry and J. D. Jacobs, pp. 105–120, Inst. of Arctic and Alp. Res. Occas. Paper No. 26, Univ. of Colorado, Boulder, Colo.

Kato, S., et al. (2011), Improvements of top-of-atmosphere and surface irradiance computations with CALIPSO-, CloudSat-, and MODIS-derived cloud and aerosol properties, *J. Geophys. Res.*, *116*, D19209, doi:10.1029/2011JD016050.

Konzelmann, T., R. S. W. van De Wal, W. Greuell, R. Bintanja, E. A. C. Henneken, and A. Abeouchi (1994), Parameterization of global and longwave incoming radiation for the Greenland ice sheet, *Global Planet. Change*, *9*, 143–164.

Lafore, J. P., et al. (1998), The meso-NH atmospheric simulation system. Part I: Adiabatic formulation and control simulations, *Ann. Geophys.*, *16*, 90–109.

Liou, K.-N. (1973), A numerical experiment on Chandrasekhar's discrete-ordinate method for radiative transfer: Applications to cloudy and hazy atmospheres, *J. Atmos. Sci.*, *30*(7), 1303–1326.
Liou, K. N., and G. D. Wittman (1979), Parameterization of the radiative properties of clouds, *J. Atmos. Sci.*, *36*, 1261–1273.
Loeb, N. G., B. A. Wielicki, D. R. Doelling, G. L. Smith, D. F. Keyes, S. Kato, N. Manalo-Smith, and T. Wong (2009), Toward optimal closure of the Earth's top-of-atmosphere radiation budget, *J. Clim.*, *22*, 748–766, doi:10.1175/2008JCLI2637.1.
Long, C. N., and T. P. Ackerman (2000), Identification of clear skies from broadband pyranometer measurements and calculation of downwelling shortwave cloud effects, *J. Geophys. Res.*, *105*(D12), 15,609–15,626, doi:10.1029/2000JD900077.
Long, C. N., J. M. Sabburg, J. Calbó, and D. Pagès (2006a), Retrieving cloud characteristics from ground-based daytime color all-sky images, *J. Atmos. Oceanic Technol.*, *23*(5), 633–652, doi:10.1175/JTECH1875.1.
Long, C. N., T. P. Ackerman, K. L. Gaustad, and J. N. S. Cole (2006b), Estimation of fractional sky cover from broadband shortwave radiometer measurements, *J. Geophys. Res.*, *111*, D11204, doi:10.1029/2005JD006475.
Marty, C., R. Philipona, J. Delamere, E. G. Dutton, J. Michalsky, K. Stamnes, R. Storvold, T. Stoffel, S. A. Clough, and E. J. Mlawer (2003), Downward longwave irradiance uncertainty under arctic atmospheres: Measurements and modeling, *J. Geophys. Res.*, *108*(D12), 4358, doi:10.1029/2002JD002937.
Maykut, G. A., and P. E. Church (1973), Radiation climate of Barrow, Alaska, 1962–1966, *J. Appl. Meteorol.*, *12*, 620–628.
Philipona, R., et al. (2001), Atmospheric longwave irradiance uncertainty: Pyrgeometers compared to an absolute sky-scanning radiometer, atmospheric emitted radiance interferometer, and radiative transfer model calculations, *J. Geophys. Res.*, *106*(D22), 28,129–28,141.
Poore, K. D., J. Wang, and W. B. Rossow (1995), Cloud layer thicknesses from a combination of surface and upper-air observations, *J. Clim.*, *8*, 550–568.
Ramanathan, V., R. D. Cess, E. F. Harrison, P. Minnis, B. R. Barkstrom, E. Ahmad, and D. Hartmann (1989), Cloud-radiative forcing and climate: Results from the Earth radiation budget experiment, *Science*, *243*, 57–63.
Ricchiazzi, P., S. Yang, C. Gautier, and D. Sowle (1998), SBDART: A research and teaching software tool for plane-parallel radiative transfer in the Earth's atmosphere, *Bull. Am. Meteorol. Soc.*, *9*, 2101–2114.
Ruckstuh, C., R. Philipona, J. Morland, and A. Ohmura (2007), Observed relationship between surface specific humidity, integrated water vapour, and longwave downward radiation at different altitudes, *J. Geophys. Res.*, *112*, D0332, doi:10.1029/2006JD007850.
Stamnes, K., S. C. Tsay, W. Wiscombe, and K. Jayaweera (1988), Numerically stable algorithm for discrete-ordinate-method radiative transfer in multiple scattering and emitting layered media, *Appl. Opt.*, *27*(12), 2502–2509.
Stephens, G. L. (1978), Radiation profiles in extended water clouds, I: Theory, *J. Atmos. Sci.*, *35*, 2111–2122.
Stephens, G. L., and P. J. Webster (1980), Clouds and climate: Sensitivity of simple systems, *J. Atmos. Sci.*, *38*, 235–247.
Stephens, G. L., J. Li, M. Wild, C. A. Clayson, N. Loeb, S. Kato, T. L'Ecuyer, P. W. Stackhouse, M. Lebsock, and T. Andrews (2012), An update on Earth's energy balance in light of the latest global observations, *Nat. Geosci.*, *5*(10), 691–696, doi:10.1038/NGEO1580.
Stubenrauch, C. J., et al. (2013), Assessment of global cloud datasets from satellites: Project and database initiated by the GEWEX radiation panel, *Bull. Am. Meteorol. Soc.*, *94*, 1031–1049, doi:10.1175/BAMS-D-12-00117.1.
Sugita, M., and W. H. Brutsaert (1993), Cloud effect in the estimation of instantaneous downward longwave radiation, *Water Resour. Res.*, *29*(3), 599–605.
Viúdez-Mora, A., J. Calbó, J. A. González, and M. A. Jiménez (2009), Modeling atmospheric longwave radiation at the surface under cloudless skies, *J. Geophys. Res.*, *114*, D18107, doi:10.1029/2009JD011885.
Wacker, S., J. Gröbner, C. Emde, L. Vuilleumier, B. Mayer, and E. Rozanov (2009), Comparison of measured and modeled nocturnal clear sky longwave downward radiation at Payerne, Switzerland. In: Current problems in atmospheric radiation (IRS 2008): Proceedings of the International Radiation Symposium (IRC/IAMAS), *AIP Conf. Proc.*, *1100*, 589–592, doi:10.1063/1.3117055.
Wacker, S., J. Gröbner, D. Nowak, L. Vuilleumier, and N. Kämpfer (2011), Cloud effect of persistent stratus nebulosus at the Payerne BSRN site, *Atmos. Res.*, *102*(1–2), 1–9.
Wacker, S., J. Gröbner, and L. Vuilleumier (2013), A method to calculate cloud-free longwave irradiance at the surface based on radiative transfer modeling and temperature lapse rate estimates, *Theor. Appl. Climatol.*, *115*, 551–561, doi:10.1007/s00704-013-0901-5.
Wang, J., and W. B. Rossow (1995), Determination of cloud vertical structure from upper-air observations, *J. Appl. Meteorol.*, *34*(10), 2443–2258.
Wang, K., and R. E. Dickinson (2013), Global atmospheric downward longwave radiation at the surface from ground-based observations, satellite retrievals, and reanalyses, *Rev. Geophys.*, *51*, 150–185, doi:10.1002/rog.20009.
Wielicki, B. A., B. R. Barkstrom, E. F. Harrison, R. B. Lee III, G. L. Smith, and J. E. Cooper (1996), Clouds and the Earth's Radiant Energy System (CERES): An Earth Observing System experiment, *Bull. Am. Meteorol. Soc.*, *77*, 853–868, doi:10.1175/1520-0477(1996)077<0853:CATERE>2.0.CO;2.
Wild, M., A. Ohmura, and U. Cubasch (1997), GCM-simulated surface energy fluxes in climate change experiments, *J. Clim.*, *10*, 3093–3110.
Zhang, J., H. Chen, Z. Li, X. Fan, and L. Peng (2010), Analysis of cloud layer structure in Shouxian, China using RS92 radiosonde aided by 95 GHz cloud radar, *J. Geophys. Res.*, *115*, 1–13, doi:10.1029/2010JD014030.
Zhou, Y., and R. D. Cess (2001), Algorithm development strategies for retrieving the downwelling longwave flux at the Earth's surface, *J. Geophys. Res.*, *106*(D12), 12,477–12,488, doi:10.1029/2001JD900144.
Zhou, Y., D. P. Kratz, A. C. Wilber, S. K. Gupta, and R. D. Cess (2007), An improved algorithm for retrieving surface downwelling longwave radiation from satellite measurements, *J. Geophys. Res.*, *112*, D15102, doi:10.1029/2006JD008159.